ACS OMEGA

Open Access

http://pubs.acs.org/journal/acsodf

Article

Phase Behavior of Hydrocarbon Fluids in Shale Reservoirs, Considering Pore Geometries, Adsorption, and Water Film

Xiaofan Chen, Liandong Tang,* Chunsheng Jia, Ping Yue, Zhenzu Zhang, and Wei Liu

Cite This: *ACS Omega* 2024, 9, 2104−2112

Read Online

ACCESS | Metrics & More | Article Recommendations

ABSTRACT: Phase behavior of hydrocarbon fluids in nanopores is different from that observed in a PVT cell due to the confinement effect. While scholars have established various models for studying the phase behavior in nanopores, the authors often ignore the effect of pore geometries, which can significantly affect the critical fluid properties in shale nanopores. In this study, we extend the Soave-Redlich-Kwong equation of state (SRK EOS) using potential theory and establish models of critical property shift, considering pore geometries, adsorption, and water film. Our research shows that the critical property shifts, considering fluid adsorption, begin at $r_p \leq 10$ nm and are seriously strengthened with nanopore radius reduction. The extended SRK EOS is applied to compute phase diagrams of the 50% C_1−50% nC_{10} mixture at different pore sizes and find that the thickness of adsorption and water film causes a depression in the P−T diagram and that the bubble point pressure is lower in cylindrical pores. At pressures above 6 MPa, the irreducible water saturation and pore geometries greatly impact the vapor−liquid ratio. This study is significant for evaluating residual oil distribution and studying fluid flow laws in shale reservoirs.

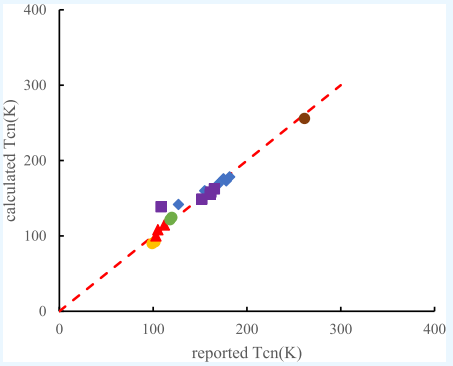

1. INTRODUCTION

In general, pores can be divided into macropores (>50 nm), mesopores (2−50 nm), and micropores (<2 nm), according to International Union of Pure and Applied Chemistry (IUPAC).[1] Shale is characterized by a prevalence of small nanopores, some of which have a radius of less than 2 nm. Pores with a radius of less than 10 nm account for up to 42% of the total pore volume.[31,32] In nanopores, the thermodynamic properties and phase behavior of confined fluids are very different from those of bulk fluids due to the confinement effect.[12] The fluid thermodynamic properties induced by the confinement effect include the critical properties, density, viscosity, surface tension, and compressibility factor of the fluid.[40,41]

Over the years, the critical property shift has been widely studied experimentally and theoretically for pure components and mixtures. Scholars measured the critical temperature of Ar, N_2, O_2, and CO_2 in MCM-41 and SBA-15 with different pore sizes.[2−9] Experimental results showed that the critical temperature in nanopores is lower than that in the bulk. On the other hand, some authors applied Grand canonical Monte Carlo (GCMC) simulation to investigate the phase behavior of confined fluid in nanopores.[10−20] The authors concluded that the critical temperature and critical pressure decrease

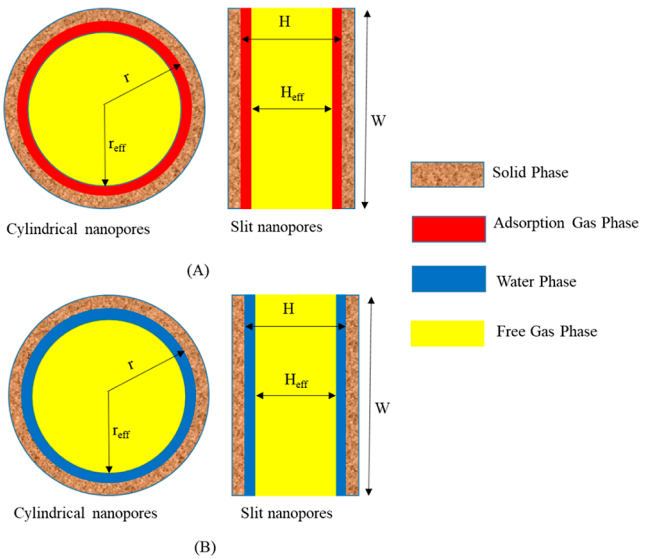

Figure 1. Diagram of the pores with different shapes. (A) organic nanopores and (B) inorganic nanopores.

Received: May 23, 2023
Revised: October 1, 2023
Accepted: October 4, 2023
Published: January 4, 2024

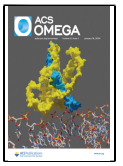

https://doi.org/10.1021/acsomega.3c03601
ACS Omega 2024, 9, 2104−2112

compared with those of the bulk, and the shift of critical properties strengthens as the pore size decreases. Based on data from physical experiments and molecular dynamics simulations, researchers established the critical property shift empirical models for confined fluids,[21−25] but the expression of these models lacks theoretical explanation. Some researchers combined Lennard-Jones potential with the equation of state to build the critical temperature and critical pressure shift equations,[26−30] but these can only be applied for cylindrical pores. The effect of the pore geometries is ignored.

According to a general classification, shale pores can be divided into organic and inorganic pores. In Figure 1, gas is adsorbed onto organic pore surfaces, forming an adsorption layer. Irreducible water is adsorbed on inorganic pore walls to form a water film.[32−34] The thickness of the adsorption layer and water film affects the effective pore radius. But the existing models that neglect these factors cannot accurately calculate the critical property shifts of confined fluid in shale reservoirs.[24−30]

Equation of state is a very convenient way to study the thermodynamic properties and phase behavior of fluids. But the classical cubic equations of state (EOS) are incapable of describing the phase behavior of confined fluids because they fail to consider the overall confinement effect.[26−30] Understanding phase behaviors and fluid thermodynamic properties is important for the production of shale reservoirs. Hence, it is imperative to develop a new phase behavior model that is suitable for shale reservoirs. Ma et al.[21] investigated the phase behavior of nanoconfined fluids in nanopores by combining PR EOS and the simplified local density (SLD) theory. Yang et al.[24] introduced a new molecule−wall interaction term, which competes with the intermolecular interaction, to extend the classical PR EOS. Song et al.[25] presented a novel way to characterize confined fluid adsorption and then developed an adsorption-dependent PR EOS. Some other models[28−30] have also been proposed to modify PR EOS by using statistical thermodynamic theory.

However, these equations of state can only be used to predict the phase behavior of confined fluids in cylindrical pores, and modifications that consider the thickness of the adsorption gas and adsorbed water layer have been sparsely seen in existing work. In this paper, the extended Soave-Redlich-Kwong equation of state (SRK EOS) is proposed with a Sutherland potential. Based on the extended SRK EOS, new critical property shift models are derived, considering the influence of pore geometries and the thickness of the adsorption gas and adsorbed water layer

2. MODEL DESCRIPTION AND ESTABLISHMENT

2.1. Extended SRK EOS. The conventional SRK EOS is modified to consider the confinement effect of the pore radius and molecule−molecule interactions in shale nanopores. The SRK EOS is one of the widely used cubic equations of state that is capable of accurately predicting fluid density. We describe confined fluids using the Sutherland potential. The canonical partition function from statistical thermodynamics is expressed as[29]

$$Q(N, V, T) = \sum_i e^{-E_i(N,V)/kT} = \frac{1}{N!}\Lambda - 3^N q_{int}^N Z(N, V, T) \quad (1)$$

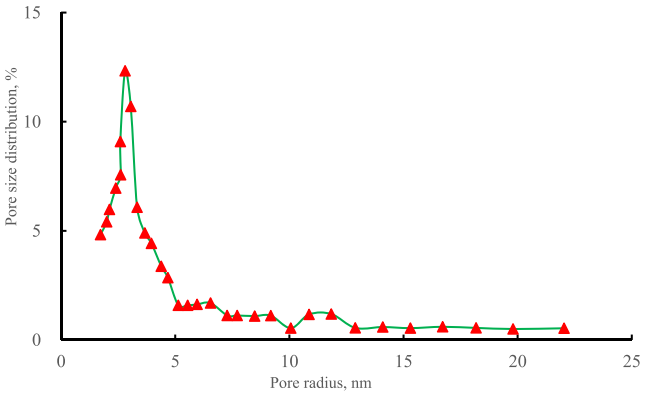

Figure 2. Pore size distribution for Barnett shale core.

where N is the number of molecules, V is the total volume, T is the temperature, E is the overall energy state, k is the Boltzmann constant, Λ is the de Broglie wavelength, $\Lambda = \left(\frac{h^2}{2\pi mkT}\right)^{0.5}$, h is the Planck's constant, m is the molecular mass, q_{int} is the internal partition function, and Z is the configuration partition function, which is shown as follows[29]

$$Z(N, V, T) = \iiint_V e^{-U(r_1, r_2, \cdots, r_N)/kT} dr_1 dr_2 \ldots dr_N \quad (2)$$

where U is the potential energy of the entire system of N number of molecules whose positions are described by r_i, i = 1, 2, 3.....N, and r_i is the distance of separation between molecules, and the pressure in nanopores can be expressed as[29]

$$P = \frac{NkT}{V - Nb} - \frac{\partial E_{conf}}{\partial V} \quad (3)$$

$$E^{conf} = \frac{kTn^2C}{2V^2} \iint_{r_i > r_o} \frac{U(r_1, r_2 \cdots r_N)}{kT} dV_1 dV_2 \quad (4)$$

Hasanzadeh[35] reported that Sutherland potential has produced more accurate results compared with Lennard-Jones to predict fluid adsorption in nanopores. Hence, we select Sutherland potential $U(r) = \begin{cases} \infty & r \le \sigma \\ -\varepsilon\left(\frac{\sigma}{R}\right)^6 & r > \sigma \end{cases}$ to describe fluid interactions and the integral part of eq 2 is solved semianalytically as

$$\frac{1}{V} \iint_{r_i > \sigma} \frac{U(r)}{kT} dV_1 dV_2 = \frac{\varepsilon\sigma^3}{kT} C(A) \quad (5)$$

where $C(A) = C_1 + \frac{C_2}{\sqrt{A}} + \frac{C_3}{A}$, $C_1 = -\frac{4\pi}{3}$, $C_2 = 7.5668$, $C_3 = -2.651$, $b = \frac{2}{3}\pi\sigma^3$, and $V = L_xL_yL_z$ We can calculate the value of C_1 by solving eq 5 analytically, and the values of C_2 and C_3 are obtained from a nonlinear least-squares method.

A is the reduced contact area. And $E_{conf}(N,V,T)$ can be expressed as

$$E_{conf} = \frac{-an2f + 2n2\varepsilon\sigma^3\left(\frac{C_2}{\sqrt{A}} + \frac{C_3}{A}\right)}{nb} \ln\left(\frac{V}{V + nb}\right) \quad (6)$$

where ε is the molecule−molecule Sutherland energy parameter and σ is the molecule−molecule Sutherland size parameter.

https://doi.org/10.1021/acsomega.3c03601
ACS Omega 2024, 9, 2104−2112

Table 1. Critical Temperature Shift of Fluid in Nanopores[a]

references	T_c (K) in bulk	fluid	r_p/nm	T_{cn} (K)	this paper	AD %	Zhang et al.[29]	AD %	Zarragoicoechea et al.[28]	AD %
Pitakbunkate et al.[18]	190.6	CH_4	2	127	141.7	11.57	165.39	30.22	158.59	24.87
			3	155	159.95	3.19	173.68	12.05	168.90	8.96
			4	169	168.29	0.42	177.87	5.24	174.19	3.07
			5	175	175.8	0.45	180.39	3.08	177.41	1.37
			6	178	173.15	2.72	182.08	2.29	179.57	0.88
			7	181.5	178.32	1.75	183.29	0.98	181.12	0.20
Vishnyakov et al.[12]			1.9	108.5	138.6	27.74	163.05	50.27	155.72	43.5
			2.28	152.0	148.89	2.04	167.55	10.23	161.27	6.09
			2.66	160.8	155.49	3.30	170.79	6.21	165.29	2.79
			2.85	161.7	158.13	2.20	172.09	6.42	166.92	3.22
			3.23	165.3	162.38	1.76	174.24	5.4	169.61	2.60
Burgess et al.[7]	304.1	CO_2	3.18	261.46	255.84	2.14	276.26	5.66	268.43	2.63
Morishige et al.[3]	154.6	O_2	1.2	102	92.1	9.7	123.98	21.54	116.4	14.11
	150.8	Ar	1.2	99	89.8	9.29	120.18	21.39	112.5	13.63
Morishige et al.[4]	126.2	N_2	3	105	108.27	3.11	115.73	10.21	112.76	7.39
			4.47	112	114.56	2.28	119.14	6.37	117.08	4.53
			2.2	103	100.1	2.81	111.99	8.72	108.08	4.93
Morishige et al.[5]	154.6	O_2	2.2	120	124.5	3.75	137.13	14.27	132.33	10.275
	150.8	Ar	2.2	118	121.43	2.90	134.36	13.86	129.68	9.89
ADD %		4.90		12.33		8.68				

[a] T_{cn} is reported literature data.

The extended SRK EOS can be obtained by substituting eq 6 into eq 3 with a specific C. The extended SRK EOS can be expressed in nanopores as

$$P = \frac{RT}{V-b} - \frac{\alpha_T\left[a_c - 0.5\varepsilon\sigma^3\left(\frac{C_2}{\sqrt{A}} + \frac{C_3}{A}\right)\right]}{V(V+b)} \tag{7}$$

2.2. Critical Properties Shift Modes. The critical temperature and pressure of the confined fluids in nanopores can be solved at the condition of $\left(\frac{\partial P}{\partial V}\right)_T = \left(\frac{\partial^2 P}{\partial V^2}\right)_T = 0$, which are derived from the modified SRK EOS in eq 7 and shown below, respectively

$$T_{cn} = \frac{3(\sqrt[3]{2}-1)^2\alpha_T}{Rb}\left[a_c - 0.5\varepsilon\sigma^3\left(\frac{C_2}{\sqrt{A}} + \frac{C_3}{A}\right)\right] \tag{8}$$

$$P_{cn} = \frac{(\sqrt[3]{2}-1)^3\alpha_T}{b^2}\left[a_c - 0.5\varepsilon\sigma^3\left(\frac{C_2}{\sqrt{A}} + \frac{C_3}{A}\right)\right] \tag{9}$$

where T_{cn} is the critical temperature in nanopores, P_{cn} is the critical temperature in nanopores, $A = \pi\left(\frac{r_{eff}}{\sigma}\right)^2$ in cylindrical nanopores, $A = \frac{\xi H_{eff}^2}{\sigma^2}$ in slit nanopores, $\xi = \frac{W}{H}$; W is height of slit nanopores, and H is width of slit nanopores.

It is well-known that corresponding the critical properties from SRK EOS are $T_c = \frac{3(\sqrt[3]{2}-1)^2\alpha_T}{Rb}$ and $P_c = \frac{(\sqrt[3]{2}-1)^3\alpha_T}{b^2}$ for bulk fluid. Therefore, the critical property shift models of confined fluid in cylindrical nanopores are shown as follows.

$$\frac{T_{cn}}{T_c} = 1 - \frac{\varepsilon\sigma^3}{2a}\left(\frac{C_2}{\sqrt{A}} + \frac{C_3}{A}\right) = 1 - 1.0194\frac{\sigma}{r_{eff}} + 0.2015\left(\frac{\sigma}{r_{eff}}\right)^2 \tag{10}$$

$$\frac{P_{cn}}{P_c} = 1 - \frac{\varepsilon\sigma^3}{2a}\left(\frac{C_2}{\sqrt{A}} + \frac{C_3}{A}\right) = 1 - 1.0194\frac{\sigma}{r_{eff}} + 0.2015\left(\frac{\sigma}{r_{eff}}\right)^2 \tag{11}$$

The critical property shift models of confined fluid in slit nanopores are shown as follows.

$$\frac{T_{cn}}{T_c} = 1 - \frac{\varepsilon\sigma^3}{2a}\left(\frac{C_2}{\sqrt{A}} + \frac{C_3}{A}\right) = 1 - \frac{1.8068\sigma}{\sqrt{\xi}H_{eff}} + \frac{0.6330}{\xi}\left(\frac{\sigma}{H_{eff}}\right)^2 \tag{12}$$

$$\frac{P_{cn}}{P_c} = 1 - \frac{\varepsilon\sigma^3}{2a}\left(\frac{C_2}{\sqrt{A}} + \frac{C_3}{A}\right) = 1 - \frac{1.8068\sigma}{\sqrt{\xi}H_{eff}} + \frac{0.6330}{\xi}\left(\frac{\sigma}{H_{eff}}\right)^2 \tag{13}$$

where $a = \frac{C_1\varepsilon\sigma^3}{2}$, r_{eff} is effective radius of cylindrical nanopores, and H_{eff} is the effective width of slit nanopores.

In Figure 2, the pore distribution is very complex in shale reservoirs. We build a simple mixing rule to the critical property shifts of mixtures in shale nanopores.

$$T_{cn} = \sum x_i y_j T_{cij} P_{cn} = \sum x_i y_j P_{cij} \tag{14}$$

where x_i is mole percentage of fluid (i) component in shale nanopores, y_j is percentage of different pore radius (j), T_{cij} is fluid (i) critical temperature in pore radius (j), and P_{cij} is fluid (i) critical pressure in pore radius (j).

2.3. Effective Pore Size. In a confined space, the fluid molecular diameter can be comparable to the pore size. Thus, the influence of the adsorption film must be considered. We assume that it is single-layer adsorption in the organic nanopores because of the presence of adsorbed gas which

https://doi.org/10.1021/acsomega.3c03601
ACS Omega 2024, 9, 2104−2112

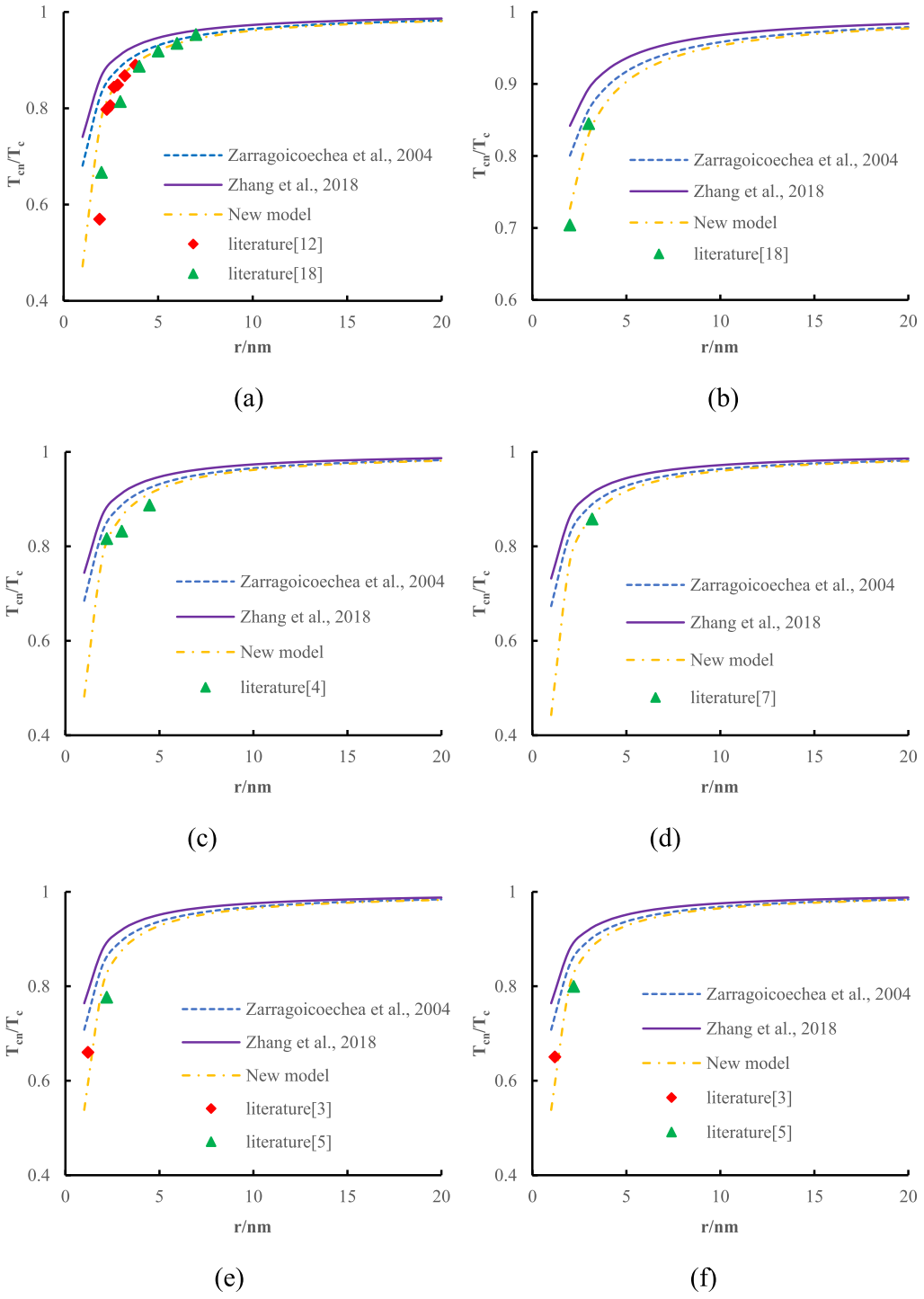

Figure 3. Measured and calculated shifts of the critical temperatures with the variations of nanopore sizes (a) CH_4 (b) C_2H_6 (c) N_2 (d) CO_2 (e) O_2 and (f) Ar.

occupies part of the space in organic nanopores. Hence, the effective radius of cylindrical nanopores and the effective width of slit nanopores can be expressed, respectively, as[36−38]

$$r_{eff} = r - d\theta \tag{15}$$

$$H_{eff} = H - 2d\theta \tag{16}$$

where θ is gas coverage on organic nanopores wall for gas, dimension less. d is the gas molecular diameter.

Irreducible water that is usually immobile is adsorbed on inorganic pore walls to form a water film. We assume that the thickness of the water film is the same. Thickness of the adsorption water film affects the effective radius. Therefore, the effective radius of cylindrical nanopores and slit nanopores can be expressed, respectively, as[39]

$$r_{eff} = r\cdot\sqrt{1 - S_{wi}} \tag{17}$$

$$H_{eff} = H\cdot(1 - S_{wi}) \tag{18}$$

where S_{wi} is irreducible water saturation.

https://doi.org/10.1021/acsomega.3c03601
ACS Omega 2024, 9, 2104−2112

3. RESULTS AND DISCUSSION

3.1. Model Verification. *3.1.1. Critical Temperature.* In Table 1, there are some experimental and molecular simulation data published.[3−5,7,12,18] Thus, we can validate the new model with experimental and molecular simulation results and compare it with the previous models directly. Figure 3 shows that the agreement between the calculated data and experimental and molecular simulation data from the new model in consideration of fluid adsorption is better than that from the previous models. Due to the confinement effect and molecule−molecule interactions, gas is adsorbed on organic pore walls to form an adsorption layer, which affects the effective pore and the vapor−liquid equilibrium. The critical property shifts considering fluid adsorption begin at $r_p \leq 10$ nm and are seriously strengthened with the nanopore radius reduction. In Figure 4 with the increase of irreducible water saturation, the thickness of the water film increases and the effective pore radius decreases. The critical property shifts strengthen with the water film increase. Therefore, it is very important to accurately calculate the critical property shift in inorganic nanopores, considering the influence of irreducible water saturation. Overall, the new model can calculate the critical property shifts of confined fluid accurately, and it can be applied in shale reservoirs.

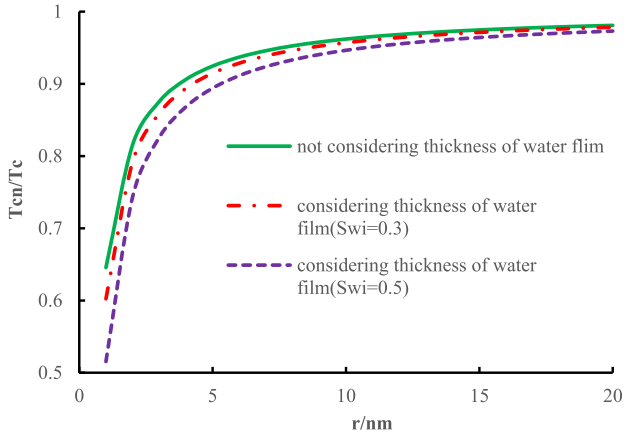

Figure 4. Critical temperature shift of methane in inorganic nanopores, considering the thickness of the water film.

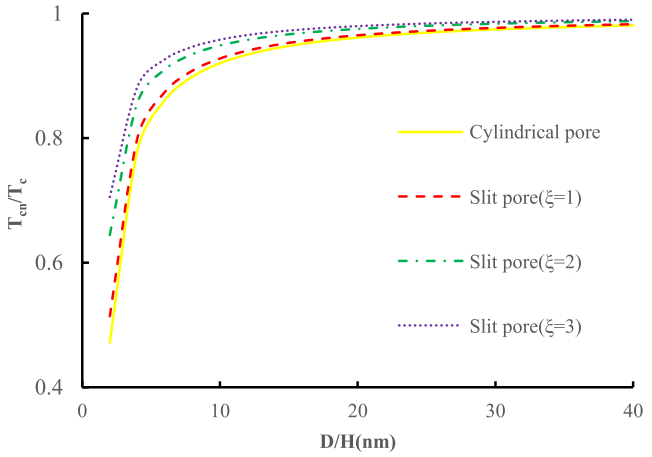

Figure 5. Critical temperature shift of methane in organic nanopores, considering adsorption; D ($D = 2r$) is cylindrical pore diameter and H is slit width.

3.2. Sensitivity Studies on Critical Properties Shift. *3.2.1. Effect of Nanopores Geometry.* Figure 5 shows that pore geometries significantly affect the fluid critical properties of shale organic nanopores. With the increase of pore size, confined fluid subjected under slit nanopores exhibits bulk behavior much earlier than that seen in cylindrical nanopores. Singh et al.[16] obtained the same conclusion by molecular dynamics simulation. With the increase of ξ, the effective space volume increases, which weakens the influence of the pore wall on the fluid. Therefore, the critical property shift is weakened. For more complex pore geometries, we will continue to study.

3.3. Sensitivity Studies on Phase Diagram. On the basis of the extended SRK EOS, the binary mixture C_1-nC_{10} was used to represent the shale reservoir fluid, and phase behavior is studied, considering pore geometries, adsorption, and water film.

3.3.1. Effect of Adsorbed Gas Thickness and Irreducible Water Saturation. Figure 6 presents the calculated phase diagrams of the binary mixture C_1-nC_{10} in nanopores by using the extended SRK EOS. The phase diagram at bulk conditions is calculated by the original SRK EOS. In the same pore radius (5 nm), the P−T diagram is depressed, considering the thickness of adsorption and water film, the critical properties became smaller, and the bubble point pressure decreased. This is because when considering the thickness of adsorption and water film, the effective pore size decreases, and the potential energy, interaction between molecules, and interaction between pore surface and molecules increase.

3.3.2. Effect of Nanopores Geometry. Figure 7 presents the phase envelope comparison of $50\%C_1-50\%nC_{10}$ mixture confined in pores of two different geometries, namely, slit and cylinder, having the same pore size ($D = 2r = 10$ nm, $H = 10$ nm). The critical properties and the bubble point pressure are lower in cylindrical pores; this clearly suggests a greater confinement effect in cylindrical pores as compared to slit pores of the same slit width. Because of the same pore size, cylindrical pores have a larger surface area and stronger interaction force. In slit pores, with the increase of ξ, the effective space volume increases, the interaction between the fluid and the fluid is more, the influence of the molecular wall is smaller, and the confinement effect is weakened.

3.4. Sensitivity Study on Vapor−Liquid Ratio of Binary Mixture. Figure 8 shows the effect of pore size on the vapor−liquid ratio in organic nanopores. At 5 nm pore radius, the molar fraction of the vapor phase is 3.34% and that of the liquid phase is 96.6%. At 10 nm pore radius, the molar fraction of the vapor phase is 10.55% and that of the liquid phase is 89.45%. In bulk, the molar fraction of the vapor phase is 14.83% and that of the liquid phase is 85.17%. With the decrease of pore size, the confinement effect is enhanced, and the vapor phase becomes the liquid phase gradually.

Therefore, in shale reservoirs, the smaller the pore size, the higher the liquid phase mole fraction.

Figures 9 and 10 show the effect of irreducible water saturation and pore geometries on the vapor−liquid ratio in inorganic nanopores. At the same pressure, the higher the irreducible water saturation, the smaller the effective pore space, the stronger the confinement effect, the smaller the vapor−liquid ratio, and the higher the liquid content in the pore. The confinement effect in cylindrical pores is stronger, and the vapor−liquid ratio is lower. At low pressure, the

https://doi.org/10.1021/acsomega.3c03601
ACS Omega 2024, 9, 2104−2112

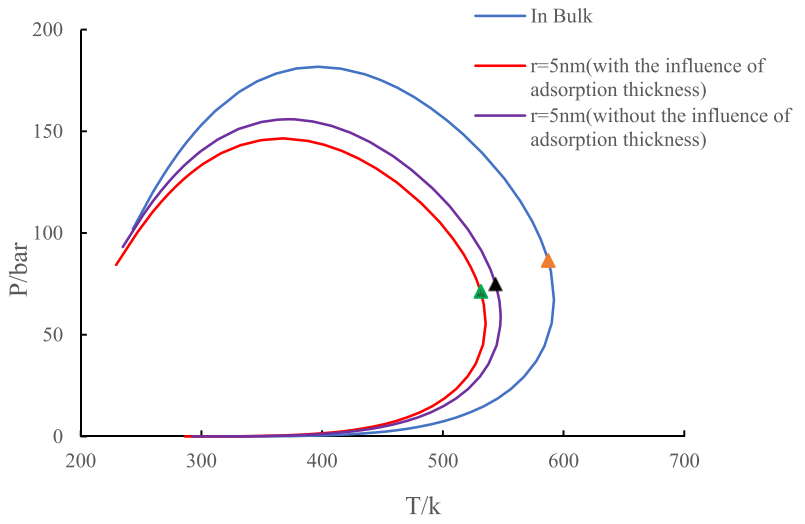

(a)

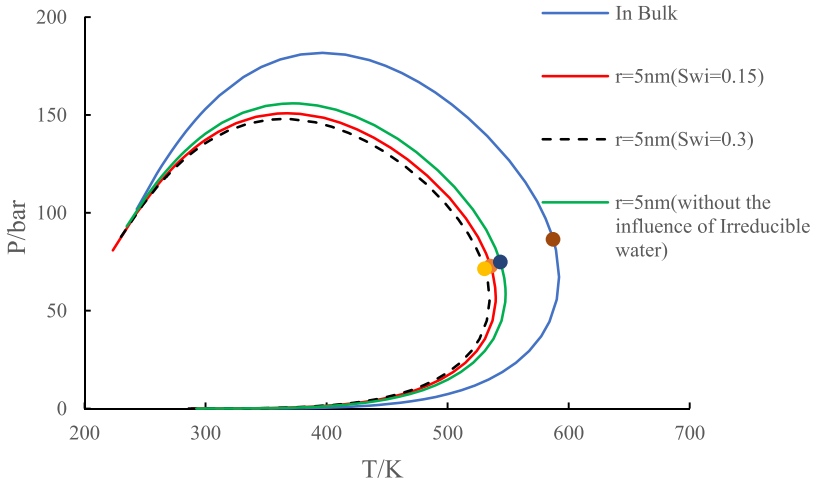

(b)

Figure 6. Phase diagram of 50%C_1−50%nC_{10} in cylindrical pores, (a) organic nanopores and (b) inorganic nanopores.

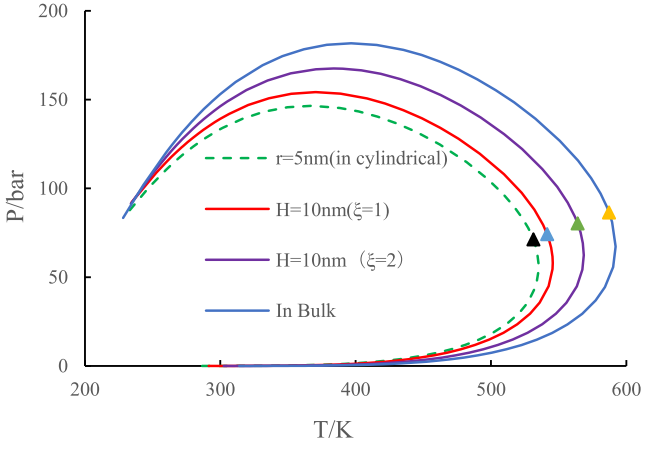

Figure 7. Phase diagram of 50%C_1−50%nC_{10}, considering pore geometries in nanopores.

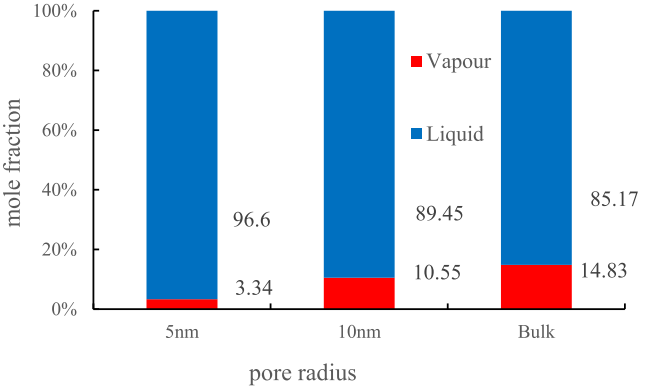

Figure 8. Effect of pore size on the vapor−liquid ratio in organic nanopores.

vapor−solid interaction between molecules is dominant, the confinement effect is weakened, and the irreducible water

https://doi.org/10.1021/acsomega.3c03601
ACS Omega 2024, 9, 2104−2112

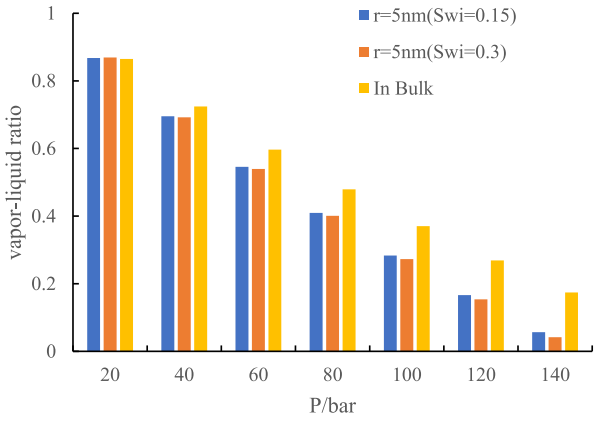

Figure 9. Effect of irreducible water saturation on the vapor−liquid ratio in inorganic nanopores.

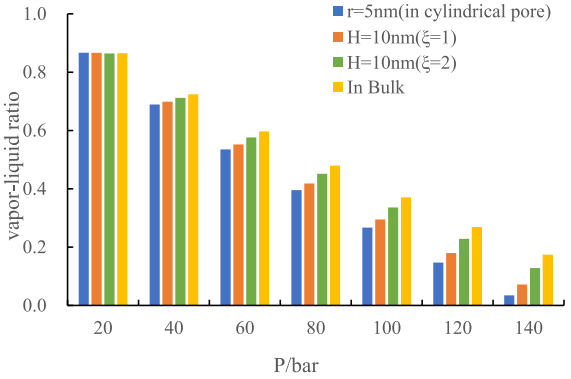

Figure 10. Effect of pore geometries on the vapor−liquid ratio in inorganic nanopores.

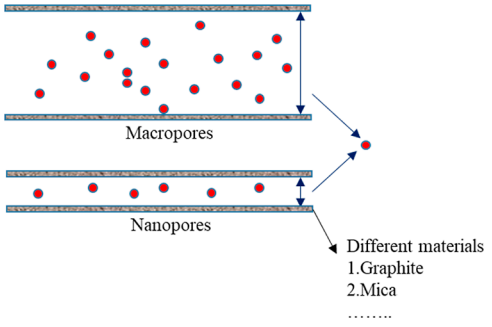

Figure 11. Molecules in different nanomaterial pores.

saturation and pore geometries have little effect on the vapor−liquid ratio. However, with the increase of pressure, at medium and high pressure, the liquid−solid interaction is dominant, confinement effect is enhanced, and the irreducible water saturation and pore geometries have a great impact on the vapor−liquid ratio. This study is of great significance for evaluating the distribution of residual oil and studying the law of fluid flow in shale reservoir.

3.5. Future Work. Compared with the previous work, the effect of pore geometries, thickness of the adsorption gas, and the adsorbed water layer on fluid phase behavior are considered in this model. However, there are still some problems to be solved in the later work (in Figure 11). First, the models ignore the effect of molecular size, as in confined space, since the molecule size is comparable to the pore size, and the molecule−wall interaction becomes strong enough to compete against the intermolecular interaction. Second, the present work has not solved the effect of nanopore materials on fluid phase behavior.

4. CONCLUSIONS

In this study, we extend the SRK EOS model to investigate the phase behavior of hydrocarbon fluids in a shale reservoir, considering pore geometries adsorption and water film. Subsequently, the P−T phase diagrams and vapor−liquid ratio of the binary mixture C_1−nC_{10} are evaluated with the proposed model. According to our study, the following conclusions can be drawn:

(1) The model can accurately describe the confined behavior of the C_1−nC_{10} mixture in nanopores with different geometries, and pore geometries significantly affect the fluid critical properties in nanopores. With the increase of pore size, the confined fluid subjected under slit nanopores closes to the bulk behavior much earlier than that seen in cylindrical nanopores.

(2) Within cylindrical or slit nanopores, the thickness of adsorbed gas and water film reduces the effective pore size, leading to a decrease in critical point and bubble point pressure. When compared to slit nanopores, cylindrical nanopores generally exhibit lower critical point and bubble point pressures despite sharing the same pore size.

(3) At low pressure, the gas−solid interaction between molecules is dominant, which weakens the confinement effect, and the irreducible water saturation and pore geometries have little effect on the vapor−liquid ratio. At medium and high pressure (P > 6 MPa), the liquid−solid interaction is dominant, the confinement effect is enhanced, and the irreducible water saturation and pore geometries have a great impact on the vapor−liquid ratio.

AUTHOR INFORMATION

Corresponding Author

Liandong Tang − *State Key Laboratory of Oil and Gas Reservoir Geology and Exploitation, Southwest Petroleum University, Chengdu 610500, China;* orcid.org/0000-0003-2452-1292; Email: 1961212289@qq.com

Authors

Xiaofan Chen − *State Key Laboratory of Oil and Gas Reservoir Geology and Exploitation, Southwest Petroleum University, Chengdu 610500, China*

Chunsheng Jia − *State Key Laboratory of Oil and Gas Reservoir Geology and Exploitation, Southwest Petroleum University, Chengdu 610500, China*

Ping Yue − *State Key Laboratory of Oil and Gas Reservoir Geology and Exploitation, Southwest Petroleum University, Chengdu 610500, China*

Zhenzu Zhang − *Huanqing Oil Production Plant of PetroChina Yumen Oilfield Branch, Jiuquan 735202 Gansu, China*

Wei Liu − *Huanqing Oil Production Plant of PetroChina Yumen Oilfield Branch, Jiuquan 735202 Gansu, China*

Complete contact information is available at: https://pubs.acs.org/10.1021/acsomega.3c03601

https://doi.org/10.1021/acsomega.3c03601
ACS Omega 2024, 9, 2104−2112

Notes

The authors declare no competing financial interest.

■ ACKNOWLEDGMENTS

This work was supported by the China Postdoctoral Science Foundation (no. 2019M650965), National Major Projects China (no.2016ZX05048-002, no. 2016ZX0501002-002), and The Fund of SKL of Oil & Gas Reservoir Geology and Exploitation Engineering (no. PLN2019020).

■ REFERENCES

(1) Rouquerol, J.; Avnir, D.; Fairbridge, C.; Everett, D.; Haynes, J.; Pernicone, N.; Ramsay, J. D. F.; Sing, K. S. W.; Unger, K. K. Recommendations for the characterization of porous solids (Technical Report). *Pure Appl. Chem.* **1994**, *66*, 1739−1758.
(2) Morishige, K.; Fujii, H.; Uga, M.; Kinukawa, D. Capillary critical point of argon, nitrogen, oxygen, ethylene, and carbon dioxide in MCM-41. *Langmuir* **1997**, *13*, 3494−3498.
(3) Morishige, K.; Shikimi, M. Adsorption hysteresis and pore critical temperature in a single cylindrical pore. *J. Chem. Phys.* **1998**, *108*, 7821−7824.
(4) Morishige, K.; Ito, M. Capillary condensation of nitrogen in MCM-41 and SBA-15. *J. Chem. Phys.* **2002**, *117*, 8036−8041.
(5) Morishige, K.; Nakamura, Y. Nature of Adsorption and Desorption Branches in Cylindrical Pores. *Langmuir* **2004**, *20*, 4503−4506.
(6) Russo, P. A.; Ribeiro Carrott, M. M. L.; Carrott, P. J. M. Trends in the condensation evaporation and adsorption enthalpies of volatile organic compounds on mesoporous silica materials. *Microporous Mesoporous Mater.* **2012**, *151*, 223−230.
(7) Burgess, C. G. V.; Everett, D. H.; Nuttall, S. Adsorption of carbon dioxide and xenon by porous glass over a wide range of temperature and pressure-applicability of the Langmuir case VI equation. *Langmuir* **1990**, *6*, 1734−1738.
(8) Kittaka, S.; Morimura, M.; Ishimaru, S.; Morino, A.; Ueda, K. Effect of confinement on the fluid properties of ammonia in mesopores of MCM-41 and SBA-15. *Langmuir* **2009**, *25*, 1718−1724.
(9) Yun, J.-H.; Düren, T.; Keil, F. J.; Seaton, N. A. Adsorption of methane, ethane, and their binary mixtures on MCM-41: Experimental evaluation of methods for the prediction of adsorption equilibrium. *Langmuir* **2002**, *18*, 2693−2701.
(10) Neimark, A. V.; Vishnyakov, A. Gauge cell method for simulation studies of phase transitions in confined systems. *Phys. Rev. E* **2000**, *62*, 4611.
(11) Vishnyakov, A.; Neimark, A. V. Multicomponent gauge cell method. *J. Chem. Phys.* **2009**, *130*, 224103.
(12) Vishnyakov, A.; Piotrovskaya, E. M.; Brodskaya, E. N.; Votyakov, E. V.; Tovbin, Y. K. Critical properties of Lennard-Jones fluids in narrow slit-shaped pores. *Langmuir* **2001**, *17*, 4451−4458.
(13) Jiang, J.; Sandler, S. I.; Smit, B. Capillary phase transitions of n-alkanes in a carbon nanotube. *Nano Lett.* **2004**, *4*, 241−244.
(14) Mota, J. P. B.; Esteves, I. A. A. C. Simplified gauge-cell method and its application to the study of capillary phase transition of propane in carbon nanotubes. *Adsorption* **2007**, *13*, 21−32.
(15) Singh, S. K.; Sinha, A.; Deo, G.; Singh, J. K. Vapor−Liquid Phase Coexistence, Critical Properties, and Surface Tension of Confined Alkanes. *J. Phys. Chem. C* **2009**, *113*, 7170−7180.
(16) Singh, S. K.; Singh, J. K. Effect of pore morphology on vapor-liquid phase transition and crossover behavior of critical properties from 3D to 2D. *Fluid Phase Equilib.* **2011**, *300*, 182−187.
(17) Pathak, M.; Cho, H.; Deo, M. Experimental and molecular modeling study of bubble points of hydrocarbon mixtures in nanoporous media. *Energy Fuels* **2017**, *31*, 3427−3435.
(18) Pitakbunkate, T.; Balbuena, P. B.; Moridis, G. J.; Blasingame, T. A. Effect of Confinement on Pressure/Volume/Temperature Properties of Hydrocarbons in Shale Reservoirs. *SPE J.* **2016**, *21*, 621−634.
(19) Jin, B.; Nasrabadi, H. Phase behavior of multi-component hydrocarbon systems in nano-pores using gauge-GCMC molecular simulation. *Fluid Phase Equilib.* **2016**, *425*, 324−334.
(20) Jin, B.; Bi, R.; Nasrabadi, H. Molecular simulation of the pore size distribution effect on phase behavior of methane confined in nanopores. *Fluid Phase Equilib.* **2017**, *452*, 94−102.
(21) Ma, Y.; Jin, L.; Jamili, A. Modifying van der Waals Equation of State to Consider Influence of Confinement on Phase Behavior. In *SPE Annual Technical Conference and Exhibition, New Orleans, Louisiana, USA*, 2013.
(22) Jin, L.; Ma, Y.; Jamili, A. Investigating the effect of pore proximity on phase behavior and fluid properties in shale formations. In *SPE Annual Technical Conference and Exhibition, New Orleans, Louisiana, USA*, 2013.
(23) Alharthy, N. S.; Nguyen, T.; Teklu, T.; Kazemi, H.; Graves, R. Multiphase compositional modeling in small-scale pores of unconventional shale reservoirs. In *SPE Annual Technical Conference and Exhibition, New Orleans, Louisiana, USA*, 2013.
(24) Yang, G.; Fan, z.; Li, X. Determination of confined fluid phase behavior using extended Peng-Robinson equation of state. *Chem. Eng. J.* **2019**, *378*, 122032.
(25) Song, Z.; Song, Y.; Guo, J.; Zhang, Z.; Hou, J. Adsorption induced critical shifts of confined fluids in shale nanopores. *Chem. Eng. J.* **2020**, *385*, 123837.
(26) Schoen, M.; Diestler, D. J. Analytical treatment of a simple fluid adsorbed in a slitpore. *J. Chem. Phys.* **1998**, *109*, 5596−5606.
(27) Zarragoicoechea, G. J.; Kuz, V. A. van der Waals equation of state for a fluid in a nanopore. *Phys. Rev. E* **2002**, *65*, 021110.
(28) Zarragoicoechea, G. J.; Kuz, V. A. Critical shift of a confined fluid in a nanopore. *Fluid Phase Equilib.* **2004**, *220*, 7−9.
(29) Zhang, K.; Jia, N.; Li, S.; Liu, L. Thermodynamic phase behaviour and miscibility of confined fluids in nanopores. *Chem. Eng. J.* **2018**, *351*, 1115−1128.
(30) Islam, A. W.; Patzek, T. W.; Sun, A. Y. Thermodynamics phase changes of nanopore fluids. *J. Nat. Gas Sci. Eng.* **2015**, *25*, 134−139.
(31) Holt, J. K.; Park, H. G.; Wang, Y.; Stadermann, M.; Artyukhin, A. B.; Grigoropoulos, C. P.; Noy, A.; Bakajin, O. Fast mass transport through sub-2-nanometer carbon nanotubes. *Science* **2006**, *312*, 1034−1037.
(32) Do, D. D.; Wang, K. A new model for the description of adsorption kinetics in heterogeneous activated carbon. *Carbon* **1998**, *36*, 1539−1554.
(33) Liu, H. L.; Wang, H. Y. Ultra-low water saturation characteristics and the identification of over-pressured play fairways of marine shales in south China. *Nat. Gas Ind.* **2013**, *33*, 140−144.
(34) Sun, Z.; Shi, J.; Wu, K.; Li, X. Gas Flow Behavior through Inorganic Nanopores in Shale Considering Confinement Effect and Moisture Content. *Ind. Eng. Chem. Res.* **2018**, *57*, 3430−3440.
(35) Hasanzadeh, M.; Alavi, F.; Feyzi, F.; Dehghani, M. R. Simplified local density model for adsorption of pure gases on activated carbon using Sutherland and Kihara potentials. *Microporous Mesoporous Mater.* **2010**, *136*, 1−9.
(36) Dong, J. J.; Hsu, J. Y.; Wu, W. J.; Shimamoto, T.; Hung, J. H.; Yeh, E. C.; Wu, Y. H.; Sone, H. Stress-dependence of the permeability and porosity of sandstone and shale from TCDP Hole-A. *J. Rock Mech. Min. Sci.* **2010**, *47*, 1141−1157.
(37) Civan, F.; Devegowda, D.; Sigal, R. F. Critical evaluation and improvement of methods for determination of matrix permeability of shale. In *SPE Annual Technical Conference and Exhibition, New Orleans, Louisiana, USA*, 2013.
(38) Wu, K.; Chen, Z.; Li, X.; Guo, C.; Wei, M. A model for multiple transport mechanisms through nanopores of shale gas reservoirs with real gas effect-adsorption-mechanic coupling. *Int. J. Heat Mass Transfer* **2016**, *93*, 408−426.
(39) Li, J.; Li, X.; Wu, K.; Feng, D.; Zhang, T.; Zhang, Y. Thickness and stability of water film confined inside nanoslits and nanocapillaries of shale and clay. *Int. J. Coal Geol.* **2017**, *179*, 253−268.

https://doi.org/10.1021/acsomega.3c03601
ACS Omega 2024, 9, 2104−2112

(40) Li, L.; Sheng, J. J. Nanopore confinement effects on phase behavior and capillary pressure in a Wolfcamp shale reservoir. *J. Taiwan Inst. Chem. Eng.* **2017**, *78*, 317−328.
(41) Wu, K.; Chen, Z. Equation of state for methane in nanoporous material at supercritical temperature over a wide range of pressure. *SPE Europec Featured at Eage Conference & Exhibition*, 2016.

https://doi.org/10.1021/acsomega.3c03601
ACS Omega 2024, 9, 2104−2112